2024 European Control Conference (ECC)
June 25-28, 2024. Stockholm, Sweden

# Multiple Time Scale Energy Management for a Fuel Cell Ship Propulsion System

Junzhe Shi, Shida Jiang, Ulf Jakob Flø Aarsnes, Dagfinn Nærheim, Scott Moura

*Abstract*— **Electrified propulsion systems, such as fuel cells (FCs) and batteries, are a promising solution to decarbonize the shipping sector. In this paper, we have conducted a comprehensive analysis of two months' worth of real-world container ship power demand data. From this analysis, we propose a novel multi-time scale Energy Management System (EMS) approach for a hybrid FC/battery propulsion system. This approach enables the individual control of each FC stack while factoring in battery and FC degradation losses and fuel consumption costs. By exploring different time scales, we have assessed the trade-offs between time complexity and system optimality, which has led us to devise an efficient strategy for the energy management of FC/battery hybrid ships.**

## I. INTRODUCTION

### A. Motivation and literature review

Amidst escalating oil prices and environmental concerns, new energy vehicles and ships powered by batteries and fuel cells (FC) are garnering increased interest due to high efficiency, extended range (relative to battery electric ships), and reduced emissions [1]. For applications like city buses [2] and ocean vessels, multiple FC stacks are required for supplying extended operating times and high transient loads [3]. It is important to find the optimal power split between each FC stack and battery pack to reduce operational costs. These operational costs include battery and FC degradation and fuel consumption costs, especially in low power operation conditions [4]. However, designing an energy management system (EMS) to manage such hybrid systems with multiple FC stacks is a challenge because multiple control actions and costs need to be considered at the same time. Moreover, the governing physics is highly nonlinear.

Various EMS control strategies aim to increase efficiency and minimize degradation, falling into optimization-based [5], rule-based, and learning-based categories [6]. Optimization-based controls, like dynamic programming (DP) in Liu et al.'s study [7], frame the EMS issue as an optimization problem. The study showed reduced hydrogen consumption by 3.10% and improved FC and battery durability by 1.08% and 0.13%, respectively. While dynamic programming guarantees global optimality, the high computational time resulting from Bellman's so-called "curse of dimensionality" hinders real-time application. Rule-based controls employ preset rules for power distribution, often tied to battery State-of-Charge (SOC), load power demand, and other parameters. They are relatively simple to interpret. Zhang et al. [8] presented a hysteresis control strategy for fuel cell plug-in hybrid vehicles, aiming to reduce FC stack switching frequency and active time. Such methods are straightforward, but generally underperform relative to optimization-based methods. Learning-based controls, like reinforcement learning (RL) exemplified by Wu et al. [9], expedite optimization-based methods by learning optimal actions through iterative interactions. However, RL methods require extensive training, potentially yielding only local or suboptimal solutions, and their reliability might waiver in untrained scenarios.

Despite growing enthusiasm for hybrid EMS design, gaps persist, notably the absence of an efficient EMS control addressing efficiency, degradation, and modular control of multiple FC stacks. In our prior research [4], we introduced an optimization-based method to control each fuel cell stack independently using Mixed Integer Quadratic Programming (MIQP). However, scaling the method to consider more FC stacks and much longer time horizons is still challenging, due to the increased computational costs. A potential solution is to use the multi-timescale model predictive control (MPC) method to overcome computational challenges. For instance, Ulbig et al. [10] employed a cascaded MPC approach for broad-scale power system control, implementing frequency control at 20 millisecond intervals and adjusting power dispatch hourly, with transmission planning spanning months to years. This strategy, seen in various studies [11] [12] [13], lessens the time complexity of the problems while maintaining rapid frequency deviation responses. By analyzing the real container ship power profile discussed in Section II.B.1), we demonstrate that similar ideas can be adopted in the FC/battery hybrid propulsion system. Specifically, we assign a longer time step interval to FC actions and a shorter time step to battery actions, motivated by the power demand analysis.

### B. Contribution

This paper develops an optimization-based EMS with reduced complexity using a multiple timescale MPC framework for FC/battery hybrid ships, inspired by our previous work in [4]. The architecture of the hybrid container ship propulsion system is presented in Fig. 1. The key contributions of this study are:

- The two-month real container ship power demand dataset is analyzed to shed light on the distribution of power demand for container ships. Furthermore, the port-to-port

*Research supported in part by NORCE under grant number 336527.
Junzhe Shi, Shida Jiang, and Scott Moura are with University of California, Berkeley, Department of Civil and Environmental Engineering, 760 Davis Hall, Berkeley, CA 94720, USA. Berkeley, CA 94720, USA (junzhe@berkeley.edu, shida_jiang@berkeley.edu, and smoura@berkeley.edu).

Ulf Jakob Flø Aarsnes is with NORCE, Postboks 22, Nygårdstangen 5838 Bergen (ulaa@norceresearch.no).

Dagfinn Nærheim is with Corvus Energy, Sandbrekketoppen 30, 5224 Nesttun, Bergen, Norway (dnaerheim@corvusenergy.com).

power profile is examined to reveal the time-frequency characteristics of container vessels.

- A multi timescale EMS for FC/battery hybrid container ships is developed to significantly reduce the computational complexity of the algorithm to make it more suitable for real-time operation.
- A comprehensive analysis of the selection of time scales and the tradeoff between time complexity and optimality is also carried out.

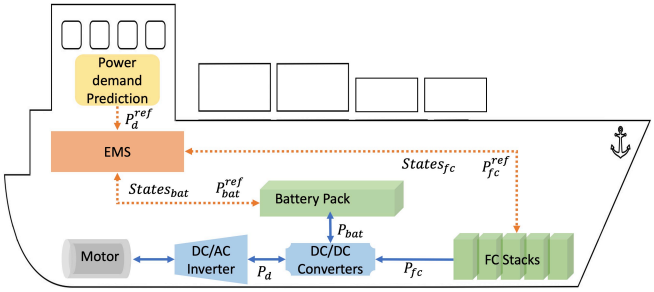


Fig. 1. Architecture of the hybrid fuel cell / battery container ship propulsion system.

### C. Organization of the Paper

The remainder of this paper is organized as follows. Section II discusses the battery and FC models used in the study. Section III performs a time-frequency analysis of a real-world container ship power profile. Section IV details the multi-timescale MPC approach. Section V presents and analyzes the simulation results of the proposed system. Finally, Section VI summarizes the key conclusions drawn from this study.

## II. Model

This section discusses the battery and FC models used for algorithm development and simulation of the test cases.

### A. Battery Model

#### 1) Battery Electrical Model

In this research, the Rint model is utilized to simulate the electrical dynamics of a battery. The schematic representation of the Rint model is depicted in Fig. 2. The dynamics of a battery can be represented by the following equations,

$$V_T = OCV + R\,I \tag{1}$$

$$P_{bat} = V_T\,I \tag{2}$$

$$I = \frac{OCV - \sqrt{OCV^2 - 4R\,P_{bat}}}{2R} \tag{3}$$

$$SOC(i) = SOC(i-1) + \frac{\Delta t\,I}{3600\,Q_{bat}} \cdot (100\%) \tag{4}$$

where $I$ is the current (in A), $OCV$ denotes the open-circuit voltage, R represents the ohmic resistance (in ohm), $V_T$ is the terminal voltage (in V), $P_{bat}$ is the power, $SOC$ is the State of Charge (in %), $\Delta t$ is the sampling time (in seconds), and $Q_{bat}$ is the nominal capacity of the battery (in Ah).

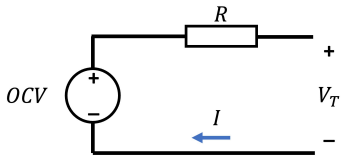


Fig. 2. Rint model of a battery.

#### 2) Battery Degradation Model

The study utilizes a degradation model for the Li-ion battery as sourced from [14]. The equations are,

$$Q_{loss} = M(C_{rate})\,exp\left(\frac{-E_a}{R\,T}\right)(Ah)^z \tag{5}$$

$$Ea = a_c + b_C\,C_{rate} \tag{6}$$

where $Q_{loss}$ represents the loss of battery capacity in percentage, $T$ is temperature, $C_{rate}$ denotes the C-rate, $Ah$ is the ampere-hour throughput, $R$ is the ideal gas constant, and $E_a$ stands for the activation energy. The parameter z represents the power law factor and is set to 0.55. The two fitting parameters, $a_c$ and $b_c$, are set at 31700 and 370.3, respectively. The parameter $M$ represents a pre-exponent factor that varies according to the C-rate.

When $Q_{loss}$ exceeds 20%, the battery is considered to have reached its end-of-life (EOL) and requires replacement. Consequently, the financial losses stemming from the battery degradation can be determined using the following equations,

$$A_{eoL} = \left(\frac{20}{M(C_{rate})\,\exp\left(\frac{-E_a}{R\,T}\right)}\right)^{\frac{1}{z}} \tag{7}$$

$$N_{eol} = \frac{3600\,A_{eoL}}{Q_{bat}} \tag{8}$$

$$L_{bat} = \frac{|I|}{2\,N_{eol}\,Q_{bat}}\Delta t\,Q_{bat}\,C_{bat} \tag{9}$$

In these equations, $A_{eoL}$ denotes the Ah throughput of the battery until its EOL, $N_{eol}$ represents the number of battery cycles until EOL, $C_{bat}$ is the price of the battery (in \$/kWh), and $L_{bat}$ is the financial loss due to battery degradation within a sampling period.

### B. Fuel Cell Model

#### 1) Power to Mass Flow Rate Curve

The relationship between the mass flow rate and the power output of a fuel cell per unit of effective catalyst surface area is derived from the Advanced Vehicle Simulator (ADVISOR), specifically from a scaled version of FC_ANL50H2. [15]. This relationship is illustrated in Fig. 3. Due to the demonstrated accuracy of quadratic functions in replicating fuel cell hydrogen consumption, as referenced in [16], a quadratic function has been used to approximate the curve that represents hydrogen consumption in correlation with the power output of the fuel cell. This is mathematically expressed as,

$$\dot{m} = a_m\,P_{fc}^2 + b_m\,P_{fc} + c_m \tag{10}$$

where $\dot{m}$ represents the mass flow rate, $P_{fc}$ denotes the output power of a fuel cell, and $a_m$, $b_m$, and $c_m$ are fitting parameters.

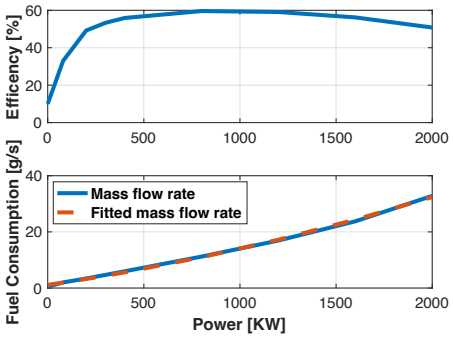


Fig. 3. [Top] Fuel cell efficiency curve. [Bottom] Fuel cell power to mass flow rate curve for a 2000 kW FC stack.

*2) Fuel Cell Degradation Model*

The degradation of a fuel cell is primarily influenced by four operational conditions: load changing, start-stop switching, idling, and high loading [17]. TABLE I presents the voltage degradation rates of the fuel cell under these four conditions. The rates of voltage drop for each condition are represented as $\Delta V_{load-change}$, $\Delta V_{on-off}$, $\Delta V_{idling}$, and $\Delta V_{high-load}$. A fuel cell is considered to have reached its end-of-life when the cumulative voltage degradation surpasses 10% of the rated voltage of a new cell. At this point, the fuel cell should be replaced due to the reduced power efficiency [18].

TABLE I
VOLTAGE DEGRADATION RATES

| Operations: | Symbols: | Drop rate: | |
|---|---|---|---|
| High power load | $\Delta V_{high-load}$ | 10μV/h | [19] |
| Idling | $\Delta V_{idling}$ | 8.66μV/h | |
| Start/Stop | $\Delta V_{on-off}$ | 0.98μV | [20] |
| Load change | $\Delta V_{load-change}$ | 1.79μV/kW | |

The financial losses (in $) associated with FC system degradation under four operating conditions, $L_{load-change}$, $L_{on-off}$, $L_{idling}$, and $L_{high-load}$, can be calculated using the voltage degradation rates provided in TABLE I as follows,

$$L_{load-change} = \frac{|\Delta P|\, \Delta V_{load-change}\, C_{fc}}{V_{drop}^{max}} \tag{11}$$

$$L_{on-off} = \begin{cases} \dfrac{\Delta V_{on-off}\, C_{fc}}{V_{drop}^{max}} & \text{if on/off triggered} \\ 0 & \text{otherwise} \end{cases} \tag{12}$$

$$L_{idling} = \begin{cases} \dfrac{\Delta t\, \Delta V_{idling}\, C_{fc}}{3600\, V_{drop}^{max}} & \text{if } 0 < P_{fc} \le P_{fc}^{low} \\ 0 & \text{if } P_{fc} > P_{fc}^{low} \end{cases} \tag{13}$$

$$L_{high-load} = \begin{cases} \dfrac{\Delta t\, \Delta V_{high-load}\, C_{fc}}{3600\, V_{drop}^{max}} & \text{if } P_{fc} \ge P_{fc}^{high} \\ 0 & \text{if } P_{fc} < P_{fc}^{high} \end{cases} \tag{14}$$

In these equations, $\Delta P$ represents the power change of the fuel cell system over the sampling period, $C_{fc}$ signifies the total cost of the fuel cell stacks (in $/kW), and $V_{drop}^{max}$ is the maximum permissible cumulative voltage drop due to degradation and is set to be 10% of the output voltage of a new fuel cell. The power thresholds, $P_{fc}^{low}$ and $P_{fc}^{high}$, are set at 20% and 80%, respectively, of the fuel cell system's maximum power supply capability [21].

## III. REAL CONTAINER SHIP POWER DATA ANALYSIS

An analysis of the power profile of container ships in this section aims to showcase the time-frequency properties and how they impact the EMS design to balance performance and computational effort.

### *A. Power distribution*

Fig. 4 illustrates the power distribution for the container ship *Sealand Balboa* over a two-month period from March 11 to May 20, 2023. Note that in 12.4% of instances, the power dips below 4000 kW. Considering the ship has a maximum power capacity of 21660 kW, power levels below 4332 kW (which is 20% of the maximum) fall into the low power range. Operating within this range can risk fuel cell inefficiency and lead to idling degradation. This can, in turn, shorten the fuel cell's lifespan and reduce its performance over time. This data underscores the importance of using individual FC stack control methods for systems with multiple FC stacks, enhancing the overall efficiency of the EMS.

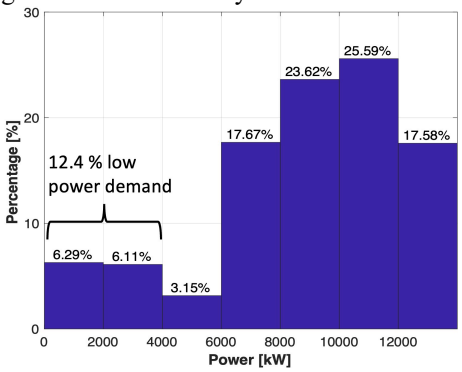


Fig. 4. The power distribution graph for the container ship *Sealand Balboa* over a two-month period.

### *B. Power profile consistency insights*

In this section, we examine the frequency distribution of the power profile, to determine the appropriate time-step for the EMS. As we shall see, the analysis motivates a multi-timescale approach. Upon closer examining the container ship port-to-port power demand profile, we note that the power consumption of the container ship is dominated by low frequency content, and specifically constant power levels. Fast Fourier Transform (FFT) is used to analyze the frequency

content of the port-to-port power profile. In Fig. 5, we can see that the large peak near the left side indicates a dominant low-frequency component in the power profile. The vast majority of frequency content is slower than $10^{-3}$ Hz.

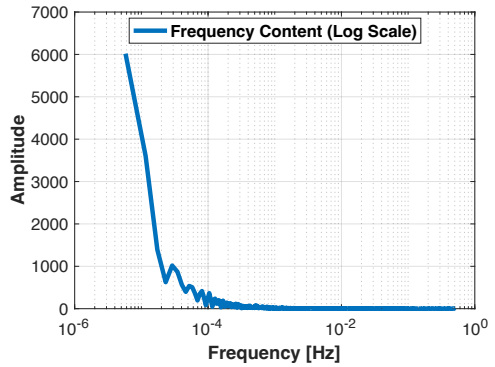


Fig. 5. The container ship port-to-port power demand profile frequency content is primarily less than $10^{-3}$ Hz.

To validate this observation, the power demand is analyzed using moving averages over varied durations, from brief 10-second intervals to more expansive 1000-second periods. The comparisons between the original power demand profile and average powers with different window durations are illustrated in Fig. 6. The Mean Absolute differences and Max Absolute differences for each window duration are detailed in TABLE II.

TABLE II
POWER DEVIATIONS FOR VARIOUS WINDOW DURATIONS

| Window Durations | Mean absolute Difference (kW) | Max Absolute Difference (kW) |
|---|---|---|
| 10 s | 81.95 | 1649.54 |
| *20 s* | 99.33 | 1787.20 |
| *60 s* | 111.68 | 2293.13 |
| *100 s* | 117.92 | 2338.85 |
| *200 s* | 126.40 | 2532.38 |
| *1000 s* | 165.49 | 4567.93 |

For instance, even when considering the broadest window duration of approximately 17 minutes (1000 s), the average power deviation from the original profile is modest, with a mean absolute difference of around 165.49 kW, less than 1% of the ship's power capacity. This observation affirms that power demands remain relatively consistent over extended periods. Therefore, it could be beneficial to use longer time intervals for the output power selection of FC stacks in the optimization process to reduce computational costs. However, it is important to consider the maximum absolute difference as well. If the time interval for the FC power update is too long, the FC's response speed will be more restricted, and the battery might struggle to bridge the gaps between the power supplied by the FC and the fluctuating power demand. From the analysis, we also derive insights for sizing hybrid energy storage systems. For instance, with the given power profile, if we allocate the average power over a 200s window duration to the FC stacks, we must ensure that the battery pack can provide at least 2532.38 kW to address the maximum absolute difference between the power supplied by the FC stacks and the actual power demand. This motivates a multi-timescale approach for this application.

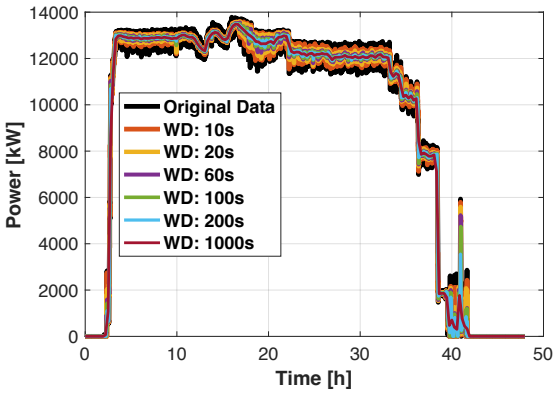


Fig. 6. Power demand profile vs. moving average outputs with different window durations (WD).

## IV. METHODOLOGY

The inherent physical dynamics of fuel cell power are more gradual compared to that of battery power. Battery voltage response is based on electrochemical kinetics, whereas fuel cells are comprised of compressors, pumps, and more. These characteristics suggest that fuel cells are well-suited to providing consistent power levels for extended periods during the optimization process. Doing so can lead to significant reductions in the computational cost. To facilitate this, we introduce the scale value, denoted as $\lambda$. This value effectively scales up the time intervals for fuel cell control actions.

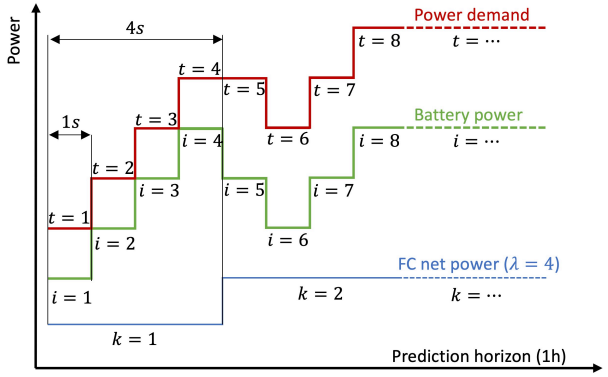


Fig. 7. Schematic representation of the multi-time scale structure, where $\boldsymbol{t}$, $\boldsymbol{i}$, and $\boldsymbol{k}$ respectively index the time steps for power demand, battery power, and FC power.

As illustrated in Fig. 7, this allows for the adjustment of the fuel cell power update frequency to be $\lambda$ times slower than its battery counterpart. Within this framework, the variable $i$ denotes the current time step for battery operations, aligning with the power demand sampling interval. Concurrently, $k$ is defined as $k = \lfloor i/\lambda \rfloor$, representing the corresponding step number for the FC operations.

The goal is to reduce degradation losses in the fuel cell stacks and battery pack, alongside minimizing hydrogen consumption costs. The objective is formulated as follows,

$$J = \sum_{i=1}^{N} l_{bat}(i) + \sum_{k=1}^{\frac{N}{\lambda}} \sum_{j=1}^{M} (\dot{m}(k,j)\ \lambda\ \Delta t\ C_{H_2} + l_{fc}(k,j)) \tag{15}$$

where, $N$ represents the total time horizon. The variable $j$ specifies a fuel cell stack, with $M$ being the total number of FC stacks. The cost associated with hydrogen consumption considers the mass fuel rate $\dot{m}(k,j)$ for a particular fuel cell stack $j$ at step $k$, time interval $\Delta t$ (seconds), and the cost of hydrogen $C_{H_2}$ ($\$/kg$). The term $l_{fc}(k,j)$ accounts for the aggregate degradation losses of the fuel cell stack $j$ at time step $k$. Meanwhile, $l_{bat}(i)$, referencing (9), captures the combined battery degradation losses.

The objective function operates within various constraints, such as power limitations, battery dynamics, and FC operational dynamics. At each time step $i$, with $k = \lfloor i/\lambda \rfloor$, the total power from all FC stacks and the battery pack must equal the power demand,

$$P_d(i) = P_{bat}(i) + \sum_{j=1}^{M} P_{fc}(k,j) \tag{16}$$

where, $P_d$ signifies the power demand, $P_{bat}$ represents the battery power output, and $P_{fc}$ denotes the power from a particular FC stack.

Using linearization methods, as detailed in [4], the battery dynamics and degradation constraints for every time step $i$ can be approximated,

$$I_{bat}(i) = a_I\ P_{bat}(i) \tag{17}$$

$$I_{bat}^{min} \le I_{bat}(i) \le I_{bat}^{max} \tag{18}$$

$$I_{bat}^{+}(i) \ge -I_{bat}(i) \tag{19}$$

$$I_{bat}^{+}(i) \ge I_{bat}(i) \tag{20}$$

$$l_{bat}(i) = \left( a_d \frac{I_{bat}^{+}(i)^2}{Q_{bat}} + b_d\ I_{bat}^{+}(i) \right) \frac{\Delta t}{7200}\ Q_{bat}\ C_{bat} \tag{21}$$

$$SOC_{bat}(i+1) = SOC_{bat}(i) + \frac{(100\%)\ \Delta t\ I_{bat}(i)}{3600\ Q_{bat}} \tag{22}$$

$$SOC_{bat}^{min} \le SOC_{bat}(i) \le SOC_{bat}^{max} \tag{23}$$

where $I_{bat}^{min}$ and $I_{bat}^{max}$ denote the lower and upper boundaries for the battery current. Additionally, $SOC_{bat}^{max}$ and $SOC_{bat}^{min}$ refer to the maximum and minimum battery SOC. The term $I_{bat}^{+}(i)$ indicates the absolute value of the battery current. The parameters, $a_I$, $a_d$ and $b_d$, are fitting parameters employed to model the nonlinear relationships between power, current, and battery degradation.

Additionally, the constraints of FC for every step $k$ and for each stack $j$ are described below,

Power limitation constraints for FC:

$$P_{fc}^{min} \le P_{fc}(k,j) \le P_{fc}^{max} \tag{24}$$

FC Mass Fuel Rate Constraints:

$$o_{fc}(k,j)\ P_{fc}^{min} \le P_{fc}(k,j) \tag{25}$$

$$P_{fc}(k,j) \le o_{fc}(k,j)\ P_{fc}^{max} \tag{26}$$

$$\dot{m}(i,j) = a_{fc}\ P_{fc}(k,j)^2 + b_{fc}\ P_{fc}(k,j) + c_{fc}\ o_{fc}(k,j) \tag{27}$$

FC Power Change Constraints:

$$\Delta P_{fc}^{+}(k,j) \ge P_{fc}(k-1,j) - P_{fc}(k,j) \tag{28}$$

$$\Delta P_{fc}^{+}(k,j) \ge P_{fc}(k,j) - P_{fc}(k-1,j) \tag{29}$$

FC degradation constraints:

$$l_{fc}(k,j) = l_{on-off}(k,j) + l_{load-change}(k,j) + l_{high-load}(k,j) + l_{idling}(k,j) \tag{30}$$

$$l_{load-change}(k,j) = \frac{\Delta V_{load-change}\ C_{fc}}{V_{drop}^{max}} \Delta P_{fc}^{+}(k,j) \tag{31}$$

$$l_{on-off}(k,j) = \frac{\Delta V_{on-off}\ C_{fc}}{V_{drop}^{max}} s_{fc}(k,j) \tag{32}$$

$$\frac{P_{fc}(k,j) - P_{fc}^{high}}{P_{fc}^{max} - P_{fc}^{high}} \le h_{fc}(k,j) \tag{33}$$

$$h_{fc}(k,j) \le \frac{P_{fc}(k,j) - P_{fc}^{min}}{P_{fc}^{high} - P_{fc}^{min}} \tag{34}$$

$$\frac{P_{fc}^{low} - P_{fc}(k,j)}{P_{fc}^{low} - P_{fc}^{min}} \le i_{fc}(k,j) \tag{35}$$

$$i_{fc}(k,j) \le \frac{P_{fc}^{max} - P_{fc}(k,j)}{P_{fc}^{max} - P_{fc}^{low}} \tag{36}$$

$$l_{idling}(k,j) = \frac{\lambda\ \Delta t\ \Delta V_{idling}\ C_{fc}\ (i_{fc}(k,j) + o_{fc}(k,j) - 1)}{3600\ V_{drop}^{max}} \tag{37}$$

$$l_{high-load}(k,j) = \frac{\lambda\ \Delta t\ \Delta V_{high-load}\ C_{fc}\ h_{fc}(k,j)}{3600\ V_{drop}^{max}} \tag{38}$$

where (27), (31), (32), (37), and (38) correspond to (10), (11), (12), (13), and (14), respectively. The lower and upper power thresholds for each a FC stack are denoted by $P_{fc}^{min}$ and $P_{fc}^{max}$. The power thresholds for idling and high-load conditions are represented by $P_{fc}^{high}$ and $P_{fc}^{low}$. The absolute value of power change is denoted by $\Delta P_{fc}^{+}(k,j)$. Four binary variables, $o_{fc}(k,j)$, $s_{fc}(k,j)$, $h_{fc}(k,j)$, and $i_{fc}(k,j)$, encode the FC

operational states such as "on", "on-off switching", "high load", and "idling" conditions, respectively.

As a result, the optimization problem is formulated as a MIQP problem. The primary decision variables are the power of each FC stack at a given time. The total number of the primary decision variables are reduced by utilizing the multiple time scale optimization structure. This adaptation allows for efficient problem-solving and enables real-time optimization capabilities.

The proposed energy management system operates as an MPC controller, wherein it actively utilizes both the predicted future power demand and the present states of the battery and FC as inputs. The prediction horizon is set to 1 hour, and the system reruns at the interval corresponding to the FC action time interval ($\lambda\,\Delta t$). During each interval, we use Gurobi [22] to solve the MIQP problem through a branch-and-bound approach. Given its MPC structure and the implementation of a multiple time scale approach (characterized by an extended FC action time interval), our system inherently mitigates the effects of zero mean predicted power demand errors and has robustness properties with respect to measurement noise and external disturbances.

## V. Results and Discussion

### A. System Setup

We tested the proposed system using a real power profile of a container ship spanning 3600 seconds with a 1-second sampling interval, depicted in Fig. 8. It represents a segment of the port-to-port power profile captured from the container ship *Sealand Balboa* on March 22, 2023. The chosen profile is particularly apt for testing due to its coverage of both the low load and high-power range, exhibiting a significant power difference of 13156 kW between its minimum and maximum values.

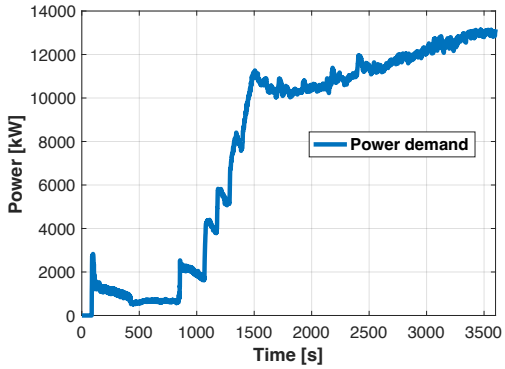


Fig. 8. The power demand profile for testing.

*Sealand Balboa* has an internal combustion propulsion system with a peak engine power output of 21660 kW. Accordingly, we consider a hybrid ship powertrain with 10 FC stacks and 1 battery pack. Here, each FC stack is capable of 2000 kW of power. Additionally, the battery pack has an energy capacity of 2500 kWh. To compute operational costs, hydrogen is priced at $4/kg. The costs for the fuel cell and battery are set at $960/kW and $178.41/kWh, respectively, according to sources [23] and [24]. The initial SOC for the battery is set at 50%. A terminal constraint is established to ensure the battery maintains a maximal reachable set for subsequent operations. Namely, the battery SOC must be greater than or equal to 50% at the end of the optimization timeframe.

### B. Comparative Analysis of Control Methods

We use the DP approach as a benchmark for evaluating our proposed algorithm's performance. Given the hybrid energy system under study, with its multiple fuel cell stacks, employing DP comes with the significant challenge of increasing computational costs, also known as the "curse of dimensionality". As the number of state variables grows, computational complexity surges. To mitigate this, the DP method treats all FC stacks as a unified entity under the "Collective Stack Control (CSC)" method, where they all receive identical control instructions. The DP method's grid sizes for SOC and fuel cell output power are defined at 1% and 200 kW. Besides, the DP time step is 1 second, which matches the time interval of the power profile. In contrast, our proposed MIQP method allows for individual control of each fuel cell stack, termed the "Individual Stack Control (ISC)" method. In the test case, we set a value of λ to 100, corresponding to a 100-second interval for FC action selection.

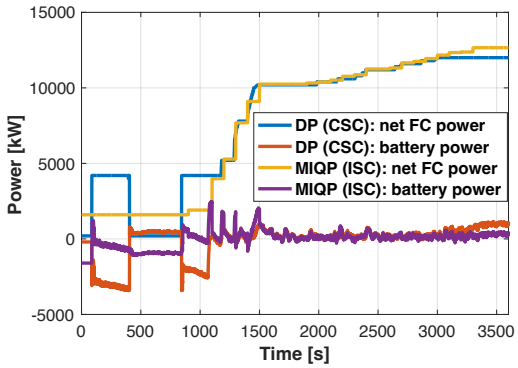


Fig. 9. Comparative power analysis between DP with the Collective Stack Control control method and the proposed MIQP method with the Individual Stack Control method.

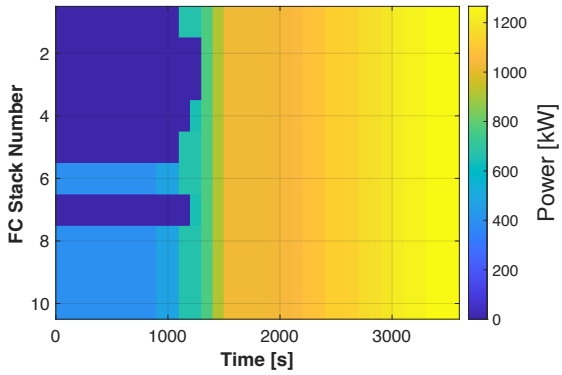


Fig. 10. Power distribution across different FC stacks using the proposed MIQP method.

As shown in Fig. 9, the power splitting between the FC and the battery is different when employing the proposed MIQP

and DP methods. The net FC power delineated in the figure represents the total power contributions from all FC stacks. While the power profiles of both methods are similar in high-power load regions, differences become obvious in the low-power load zones. This difference arises from our proposed method's capability to independently control each FC stack. This individual control permits the shutdown of redundant FC stacks, avoiding FC idling degradation losses and ensuring optimal fuel efficiency, thus minimizing FC degradation and fuel consumption costs. The powers across individual FC stacks are shown in Fig. 10. Notice the power levels are non-uniform at low demand periods.

Comparative findings between DP and our proposed method for λ=100 are summarized in TABLE III. Notably, despite activating stacks 1-5 and 7, which leads to additional on-off switch loss, our method achieves a total cost that is 12.72% less than DP. This outcome highlights the advantages of adopting an ISC approach over the CSC approach. Additionally important, the computational speed of our proposed algorithm is 136x times faster than the DP method, even with individual FC stack control.

TABLE III
COMPARISON METRICS BETWEEN DP AND PROPOSED METHOD

| | DP | Proposed Method ($\lambda = 100$) |
|---|---|---|
| Battery degradation loss ($) | 102.5907 | 32.3721 |
| H2 consumption cost ($) | 1635.2 | 1599.2 |
| FC idling loss ($) | 242.9 | 0 |
| FC high load loss ($) | 0 | 0 |
| FC load change loss ($) | 48.6 | 26.6 |
| FC on/off switch loss ($) | 0 | 112.9 |
| Total cost ($) | 2029.3 | 1771.1 |
| Total computational time (s) | 9492.7 | 69.7 |

### C. *Investigation of the scale size*

We conducted tests on our proposed system using different (time) scale values to observe their impacts on total cost and computational time. Our findings are presented in Fig. 11, which shows that there is a correlation between scale value and total cost. As the scale value $\lambda$ increases, there is a gradual increase in total cost. However, we also observed that there is a significant decrease in computational time with increasing scale value. Due to the consistency of the container ship's power profile, the increase in total cost is not as significant as the reduction in computational time. For example, by changing the scale value from $\lambda = 10$ to $\lambda = 100$, we saw only a slight 0.24% increase in total cost. However, the computational time reduced to one-tenth of its original duration. These results demonstrate the benefits of using a multi-timescale EMS approach, which improves computational efficiency and enables real-time operation while remaining close to optimal outcomes.

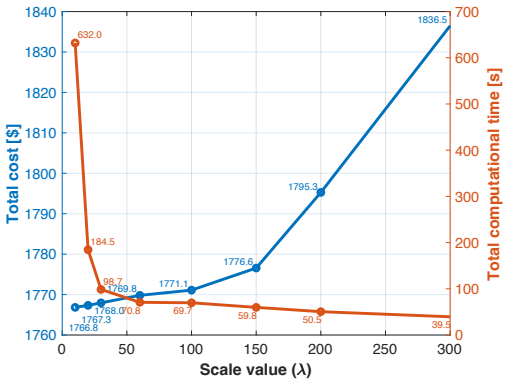

Fig. 11. Scale value vs. Total cost and Total computational time.

It is important to note, however, that increasing the scale value arbitrarily is not feasible. If the scale value is set too high, it may cause an FC stack to remain unchanged for an extended period, leading to an infeasible optimization result in the presence of sudden and large changes in demand. This is because the battery may not be able to handle the power difference due to its SOC and current constraints. This motivates adjusting the scale value dynamically during operation. For instance, a smaller scale value should be used during sailing and berthing when sudden and significant power changes may occur. This can ensure optimization feasibility and achieve low total cost. Conversely, higher scales can be used when power remains relatively consistent to save computational resources.

## VI. CONCLUSION

Through detailed analysis of a real container ship power demand dataset, our study found that 12.4% of operations fall into the low power demand category. Additionally, we discerned a pronounced consistency in the power consumption time signal for container ships. This characteristic of the power demand profile provided the foundation for our multi-time scale optimization algorithm. Leveraging this consistency, our method assigns longer step intervals to FC actions, thereby reducing computational complexity while ensuring the system's efficiency. Compared to the DP method employing the Collective Stack Control approach, our proposed system, which uses the Individual Stack Control approach with λ=100, achieved a 12.72% cost reduction and operated at a computational speed that was 136x faster.

Given its efficiency and adaptability, we find the multi-time scale EMS approach is promising for overcoming the tradeoff between performance and computational complexity, with potential applications in other large-scale transportation modes. A practical challenge of applying this approach in real-world scenarios is the requirement for prior knowledge of the power demand profile. Therefore, future research could investigate methods for predicting power demand or aim to design a system that optimizes sailing speed, thereby directly offering an optimized future power demand profile.

## REFERENCES


[1] F. Ustolin, N. Paltrinieri, and F. Berto, "Loss of integrity of hydrogen technologies: A critical review," *International Journal of Hydrogen Energy*, vol. 45, no. 43, pp. 23809–23840, Sep. 2020, doi: 10.1016/j.ijhydene.2020.06.021.

[2] J. Shi, B. Xu, Y. Shen, and J. Wu, "Energy management strategy for battery/supercapacitor hybrid electric city bus based on driving pattern recognition," *Energy*, p. 122752, Nov. 2021, doi: 10.1016/j.energy.2021.122752.

[3] J. Ling-Chin *et al.*, "Technology roadmap for hydrogen-fuelled transportation in the UK," *International Journal of Hydrogen Energy*, Apr. 2023, doi: 10.1016/j.ijhydene.2023.04.131.

[4] J. Shi, U. J. F. Aarsnes, D. Nærheim, and S. Moura, "Online energy management system for a fuel cell/battery hybrid system with multiple fuel cell stacks." arXiv, Oct. 19, 2023. doi: 10.48550/arXiv.2310.13208.

[5] J. Shi, B. Xu, X. Zhou, and J. Hou, "A cloud-based energy management strategy for hybrid electric city bus considering real-time passenger load prediction," *Journal of Energy Storage*, vol. 45, p. 103749, Jan. 2022, doi: 10.1016/j.est.2021.103749.

[6] B. Xu, J. Shi, S. Li, H. Li, and Z. Wang, "Energy consumption and battery aging minimization using a Q-learning strategy for a battery/ultracapacitor electric vehicle," *Energy*, vol. 229, p. 120705, Aug. 2021, doi: 10.1016/j.energy.2021.120705.

[7] Y. Liu, J. Liang, J. Song, and J. Ye, "Research on Energy Management Strategy of Fuel Cell Vehicle Based on Multi-Dimensional Dynamic Programming," *Energies*, vol. 15, no. 14, Art. no. 14, Jan. 2022, doi: 10.3390/en15145190.

[8] A. Macias Fernandez, M. Kandidayeni, L. Boulon, and H. Chaoui, "An Adaptive State Machine Based Energy Management Strategy for a Multi-Stack Fuel Cell Hybrid Electric Vehicle," *IEEE Transactions on Vehicular Technology*, vol. 69, no. 1, pp. 220–234, Jan. 2020, doi: 10.1109/TVT.2019.2950558.

[9] P. Wu, J. Partridge, and R. Bucknall, "Cost-effective reinforcement learning energy management for plug-in hybrid fuel cell and battery ships," *Applied Energy*, vol. 275, p. 115258, Oct. 2020, doi: 10.1016/j.apenergy.2020.115258.

[10] A. Ulbig, M. Arnold, S. Chatzivasileiadis, and G. Andersson, "Framework for Multiple Time-Scale Cascaded MPC Application in Power Systems," *IFAC Proceedings Volumes*, vol. 44, no. 1, pp. 10472–10480, Jan. 2011, doi: 10.3182/20110828-6-IT-1002.01859.

[11] C. Liu, C. Wang, Y. Yin, P. Yang, and H. Jiang, "Bi-level dispatch and control strategy based on model predictive control for community integrated energy system considering dynamic response performance," *Applied Energy*, vol. 310, p. 118641, Mar. 2022, doi: 10.1016/j.apenergy.2022.118641.

[12] A. Valibeygi, S. A. R. Konakalla, and R. de Callafon, "Predictive Hierarchical Control of Power Flow in Large-Scale PV Microgrids With Energy Storage," *IEEE Transactions on Sustainable Energy*, vol. 12, no. 1, pp. 412–419, Jan. 2021, doi: 10.1109/TSTE.2020.3001260.

[13] E. Mayhorn, L. Xie, and K. Butler-Purry, "Multi-Time Scale Coordination of Distributed Energy Resources in Isolated Power Systems," *IEEE Transactions on Smart Grid*, vol. 8, no. 2, pp. 998–1005, Mar. 2017, doi: 10.1109/TSG.2016.2547342.

[14] J. Wang *et al.*, "Cycle-life model for graphite-LiFePO4 cells," *Journal of Power Sources*, vol. 196, no. 8, pp. 3942–3948, Apr. 2011, doi: 10.1016/j.jpowsour.2010.11.134.

[15] T. Markel *et al.*, "ADVISOR: a systems analysis tool for advanced vehicle modeling," *Journal of Power Sources*, vol. 110, no. 2, pp. 255–266, Aug. 2002, doi: 10.1016/S0378-7753(02)00189-1.

[16] F. Odeim, J. Roes, L. Wülbeck, and A. Heinzel, "Power management optimization of fuel cell/battery hybrid vehicles with experimental validation," *Journal of Power Sources*, vol. 252, pp. 333–343, Apr. 2014, doi: 10.1016/j.jpowsour.2013.12.012.

[17] P. Pei, Q. Chang, and T. Tang, "A quick evaluating method for automotive fuel cell lifetime," *International Journal of Hydrogen Energy*, vol. 33, no. 14, pp. 3829–3836, Jul. 2008, doi: 10.1016/j.ijhydene.2008.04.048.

[18] Y. Wang, S. J. Moura, S. G. Advani, and A. K. Prasad, "Power management system for a fuel cell/battery hybrid vehicle incorporating fuel cell and battery degradation," *International Journal of Hydrogen Energy*, vol. 44, no. 16, pp. 8479–8492, Mar. 2019, doi: 10.1016/j.ijhydene.2019.02.003.

[19] H. Chen, P. Pei, and M. Song, "Lifetime prediction and the economic lifetime of Proton Exchange Membrane fuel cells," *Applied Energy*, vol. 142, pp. 154–163, Mar. 2015, doi: 10.1016/j.apenergy.2014.12.062.

[20] K. Song, H. Chen, P. Wen, T. Zhang, B. Zhang, and T. Zhang, "A comprehensive evaluation framework to evaluate energy management strategies of fuel cell electric vehicles," *Electrochimica Acta*, vol. 292, pp. 960–973, Dec. 2018, doi: 10.1016/j.electacta.2018.09.166.

[21] Y. Zhou, A. Ravey, and M.-C. Péra, "Real-time cost-minimization power-allocating strategy via model predictive control for fuel cell hybrid electric vehicles," *Energy Conversion and Management*, vol. 229, p. 113721, Feb. 2021, doi: 10.1016/j.enconman.2020.113721.

[22] "Gurobi Optimizer Reference Manual," Gurobi Optimization. Accessed: Jul. 13, 2023. [Online]. Available: https://www.gurobi.com/documentation/current/refman/index.html

[23] S. Di Micco, L. Mastropasqua, V. Cigolotti, M. Minutillo, and J. Brouwer, "A framework for the replacement analysis of a hydrogen-based polymer electrolyte membrane fuel cell technology on board ships: A step towards decarbonization in the maritime sector," *Energy Conversion and Management*, vol. 267, p. 115893, Sep. 2022, doi: 10.1016/j.enconman.2022.115893.

[24] K. Li, J. Zhou, C. Jia, F. Yi, and C. Zhang, "Energy sources durability energy management for fuel cell hybrid electric bus based on deep reinforcement learning considering future terrain information," *International Journal of Hydrogen Energy*, Jun. 2023, doi: 10.1016/j.ijhydene.2023.05.311.